In *nifV*⁻ strains *homo*citrate may be replaced by the common metabolite citrate during the biosynthesis of the cofactor.[8c] We speculate that the additional exchangeable proton detected in the ^{1}H ENDOR of *nifV*⁻ protein may be on a water molecule present in a cavity that owes its existence to the replacement of *homo*citrate by citrate, either as a template ligand during cofactor biosynthesis or as a component (or component precursor) in the finished cofactor entity.

Acknowledgment. This work was supported by Grants DMB89-07559 (B.M.H.) and DMB85-20687 (W.H.O.-J.) from the National Science Foundation Biophysics Program and by Grant 87-CRCR-1-2430 from the USDA (B.M.H.). The ENDOR spectrometer was purchased with a grant from the NSF Biological Instrumentation Program (PCM-8116106) and received support from the National Institutes of Health (HL-13531, B. M.H.) and the Northwestern University Materials Research Center under the NSF-MRC Program (DMR 8216972).

Registry No. FeMoCO, 72994-52-6; Fe, 7439-89-6; Mo, 7439-98-7.

NMR Studies of the Dinuclear Iron Site in Reduced Uteroferrin and Its Oxoanion Complexes

Robert C. Scarrow, Joseph W. Pyrz, and Lawrence Que, Jr.*

Contribution from the Department of Chemistry, University of Minnesota, 207 Pleasant St. S.E., Minneapolis, Minnesota 55455. *Received December 19, 1988*

Abstract: The chemical shifts and relaxation behavior of paramagnetically shifted proton NMR resonances of reduced uteroferrin (Uf_r) and its XO_4^{n-} complexes ($n = 2$: X = Mo, W; $n = 3$: X = P, As) are reported. Integrations with respect to an internal standard show that downfield resonances ($\delta > 14$ ppm vs TMS) arise from 10 protons on ligands to the paramagnetic dinuclear iron center of Uf_r and upfield resonances ($\delta < -10$ ppm vs TMS) arise from at least two protons. Two downfield and one upfield resonance are lost in D_2O. Binding of molybdate, tungstate, or arsenate of Uf_r at pH 4.9 causes minor changes in δ, whereas anaerobic addition of phosphate results in loss of interpretable NMR signals outside of the −3 to 15 ppm range. Uf_rPO_4 at pH 3 exhibits downfield-shifted resonances somewhat larger than those of the other oxoanion complexes at pH 4.9, which suggests weaker antiferromagnetic coupling in Uf_rPO_4. Primarily on the basis of δ and T_1 values, seven of the paramagnetically shifted resonances are assigned to a single tyrosine bound to iron(III) and to a histidine bound to each of the two iron atoms. Probable assignments are given for other paramagnetically shifted peaks.

Uteroferrin is a glycoprotein of molecular weight 40 000 isolated from porcine uteri.[1,2] It is abundantly present in the allantoic fluid of pregnant sows and can also be isolated in high yield (up to 0.5 g per pig) from progesterone-treated gilts.[3] Uteroferrin exhibits phosphatase activity with maximal activity at pH 5 and, unlike many phosphatases, it is not inhibited by tartrate. These properties and its color establish uteroferrin as a member of the "purple acid phosphatases", which have been found in many mammalian species (including humans) as well as in yeast and plants.[4] The mammalian enzymes contain a dinuclear iron center per protein molecule,[5,6] while active preparations of various plant enzymes have been reported to have manganese,[7] iron,[8] and dinuclear iron-zinc centers.[9]

Enzymatically active uteroferrin (Uf_r) contains an antiferromagnetically coupled dinuclear iron center in the mixed-valence oxidation state. The Mössbauer spectrum of Uf_r demonstrates the presence of one ferrous and one ferric ion in each protein molecule,[10] and the low-temperature EPR spectrum of Uf_r consists of signals with principal g values of 1.93, 1.74, and 1.59, indicative of an $S = {}^1/_2$ ground state arising from an antiferromagnetically coupled Fe(II)-Fe(III) spin system.[5] Magnetic susceptibility measurements indicate a coupling constant between the high-spin metal centers of $2J = -19.8 \pm 0.5$ cm^{-1} (for $\mathcal{H} = -2J\mathbf{S}_1\cdot\mathbf{S}_2$).[11]

The visible spectrum of Uf_r consists of a broad feature centered at 510 nm, which is assigned to a tyrosinate-to-iron(III) charge-transfer band by resonance Raman spectroscopy.[12] The comparatively large extinction coefficient of uteroferrin (4000 M^{-1} cm^{-1}) and multiple peaks observed in the visible circular dichroism spectra of both oxidation states of uteroferrin led to the suggestion that two tyrosines are bound to the iron, which remains trivalent in both Uf_r and Uf_o.[5]

Uf_r can bind a variety of oxoanions.[13] Molybdate or tungstate are tightly bound inhibitors ($K_i \approx 4$ μM)[14] of uteroferrin and stabilize the mixed-valence oxidation state. Phosphate and arsenate, on the other hand, are more weakly bound inhibitors (K_i's in the millimolar range)[14] and facilitate the air oxidation of Uf_r.[5,13] We have shown that these latter anions form Uf_r-anion complexes[15] prior to their aerobic conversion to the oxidized anion complex over the course of several hours. The oxoanions affect the spectroscopic properties of uteroferrin[13] and are of interest as models of enzyme-substrate and enzyme-product complexes of the catalytic cycle.

We have previously reported NMR studies of Uf_o and Uf_r. While Uf_r exhibited well-resolved paramagnetically shifted resonances, Uf_o exhibited no resonances outside the diamagnetic region.[16] In the present paper we report NMR spectra for several

(1) Chen, T. T.; Bazer, F. W.; Cetorelli, J. J.; Pollard, W. E.; Roberts, R. M. *J. Biol. Chem.* **1973**, *248*, 8560-8566.
(2) Baumbach, G. A.; Ketcham, C. M.; Richardson, D. E.; Bazer, F. W.; Roberts, R. M. *J. Biol. Chem.* **1986**, *261*, 12869-12878.
(3) Basha, S. M. M.; Bazer, F. W.; Geisert, R. D.; Roberts, R. M. *J. Anim. Sci.* **1980**, *50*, 113-123.
(4) Antanaitis, B. C.; Aisen, P. *Adv. Inorg. Biochem.* **1983**, *5*, 111-136.
(5) Antanaitis, B. C.; Aisen, P.; Lilienthal, H. R. *J. Biol. Chem.* **1983**, *258*, 3166-3172.
(6) Averill, B. A.; Davis, J. C.; Berman, S.; Zirino, T.; Sanders-Loehr, J.; Loehr, T. M.; Sage, J. T.; Debrunner, P. G. *J. Am. Chem. Soc.* **1987**, *109*, 3760-3767.
(7) Kawabe, H.; Sugiura, Y.; Terauchi, M.; Tanaka, H. *Biochim. Biophys. Acta* **1984**, *784*, 81-89.
(8) Hefler, S. K.; Averill, B. A. *Biochem. Biophys. Res. Commun.* **1987**, *146*, 1173-1177.
(9) Beck, J. L.; de Jersey, J.; Zerner, B.; Hendrich, M. P.; Debrunner, P. G. *J. Am. Chem. Soc.* **1988**, *110*, 3317-3318.
(10) Debrunner, P. G.; Hendrich, M. P.; De Jersey, J.; Keough, D. T; Sage, J. T.; Zerner, B. *Biochim. Biophys. Acta* **1983**, *745*, 103-106.
(11) Day, E. P.; David, S. S.; Peterson, J.; Dunham, W. R.; Bonvoisin, J.; Sands, R. H.; Que, L., Jr. *J. Biol. Chem.* **1988**, *263*, 15561-15567.
(12) (a) Gaber, B. P.; Sheridan, J. P.; Bazer, F. W.; Roberts, R. M. *J. Biol. Chem.* **1979**, *254*, 8340-8342. (b) Antanaitis, B. C.; Strekas, T.; Aisen, P. *J. Biol. Chem.* **1982**, *257*, 3766-3770.
(13) Antanaitis, B. C.; Aisen, P. *J. Biol. Chem.* **1985**, *260*, 751-756.
(14) Pyrz, J. W. Ph.D. Dissertation, Cornell University, Ithaca, NY, 1986.
(15) Pyrz, J. W.; Sage, J. T.; Debrunner, P. G.; Que, L., Jr. *J. Biol. Chem.* **1986**, *261*, 11015-11020.

0002-7863/90/1512-657$02.50/0

oxoanion complexes of Uf_r as well as relaxation times and integrations relative to an internal standard for many of the paramagnetically shifted resonances. The new data give additional information on the number and identity of the amino acid ligands to the dinuclear iron center in reduced uteroferrin, as well as indications of conformational changes upon oxoanion binding.

Experimental Section

Purification of Uteroferrin. Uteroferrin was isolated and purified from the uteri of gilts treated with 1,3,5(10)-estradiol-3,17β-diol 17-valerate. The procedure used has been previously described.[3,15] The purity of the uteroferrin was judged both by its optical spectrum (A_{280}/A_{510} = 13–14) and by its activity in hydrolyzing 10 mM *p*-nitrophenyl phosphate at pH 4.9.[17] Freshly prepared uteroferrin exhibited specific activities of 400–500 μmol/min·mg without pretreatment with reducing agents (such as β-mercaptoethanol); however, upon standing several weeks at 4 °C, the visible λ_{max} red-shifted and the specific activity decreased due to autoxidation. This could be reversed by treatment of the sample with β-mercaptoethanol and catalytic amounts of iron(II) salts.[15]

Uteroferrin Anion Complexes. The tungstate and molybdate complexes of uteroferrin are routinely prepared by addition of a solution of 1.1 molar equiv of Na_2XO_4 (X = Mo, W) to dilute (<0.1 mM) solutions of uteroferrin followed by enzyme concentration. The air-sensitive arsenate and phosphate complexes were prepared by anaerobic addition of buffered oxoanion solutions to concentrated protein solution to give ca. 100 mM arsenate or phosphate at the desired final pH. Except where noted, spectra were obtained in pH 4.9 buffer (0.1 M NaOAc/HOAc, 0.2 M NaCl). The D_2O-based buffers were prepared with a mole ratio of NaOAc to DOAc of 2:1 (the same as the NaOAc/HOAc ratio used to prepare pH 4.9 buffer).

NMR Spectra. Spectra were obtained at 300 MHz with a Nicolet NT-300 spectrometer using a 5-mm proton probe. Temperature control was provided by a TRI Research T-2000 Cryo Controller. The sample temperature was determined from the chemical shift difference between the peaks of a MeOH/0.1% HCl sample by the equation of Van Geet.[18] Chemical shift values are reported relative to the H_2O or HOD resonance at 4.8 ppm, with positive values indicating downfield shifts. Reported peak widths have been corrected for line broadening introduced by exponential apodization of the FID (usually 50 Hz for uteroferrin spectra).

NMR spectra described in this paper were obtained with modifications of the inversion–recovery pulse sequence $(180°_x-\tau-90°_y-t_{FID}-t_{delay})_n$ using quadrature-phase cycling. The 180° pulse (ca. 10 μs) was replaced by a $90°_x-240°_y-90°_x$ composite pulse to provide more effective inversion over the ca. ±40 KHz spectral range.[19] Due to the submillisecond T_2 values of the shifted Uf_r resonances, true 180° inversions is not critical, the t_{FID} values of 20–50 ms are sufficient. Initial observation of the paramagnetically shifted (and relaxed) resonances in H_2O was accomplished by the "super-WEFT" technique[20] of rapid pulsing (t_{delay} = 0) to partially saturate slowly relaxing peaks (most resonances of Uf_r lie between −3 and 12 ppm and have T_1 values of approximately 500 ms) and then nulling the H_2O signal by the choice of τ (typically to a value 70–90% of t_{FID}).

For determination of T_1 values and integrations of protein samples, $t_{FID} + t_{delay}$ was set to 125 or 150 ms to ensure complete relaxation of the paramagnetically shifted resonances between pulses. For T_1 studies in H_2O, the water signal was suppressed by irradiation during τ and t_{delay}. To minimize the effects of temperature and amplifier gain drift, sums of FIDs were saved for n = 512 or 1024 for each of the 13–16 τ values (between 1 and 120 ms; arranged nonconsecutively), after which the process was repeated ~10 times and the data were subsequently averaged; overall data collection required ~8 h. The same phase parameters were used for all spectra in the T_1 determination data set. A linear base-line correction was applied to sections of the spectrum from which peak positions, widths, and amplitudes were determined by use of the spectral simulation program NMCCAP of the Nicolet NMR software package. Each spectrum was simulated in order to leave a difference (obs − calc) spectrum with no visually apparent peaklike features; however, the difference spectrum normally includes the slow base-line roll resulting from nonlinear response of the receiver during the first 50 μs after the RF pulse and could include very broad peaks from protons less than ca. 4 Å from the iron atoms. The rolling base line is evident in Figure 1. For measurement of chemical shifts (as in the studies of δ vs temperature) and in preparation of Figures 3 and 4, a cubic spline base-line correction was applied to the phase-corrected spectra; such corrections were not applied to spectra from which widths or heights of peaks were measured.

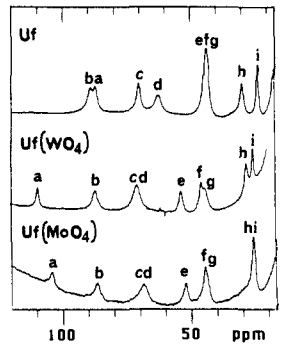

Figure 1. Downfield region of 300-MHz ^1H NMR spectra of Uf_r, Uf_rMoO_4, and Uf_rWO_4 obtained at 31 °C and pH 4.9. These spectra were obtained by the super-WEFT technique and have not been base-line corrected.

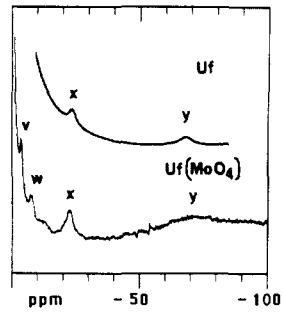

Figure 2. Upfield region of 300-MHz ^1H NMR spectra of Uf_r and Uf_rMoO_4 obtained at 31 °C and pH 4.9. A linear tilt base-line correction has been applied to each spectrum.

For T_1 measurements on model compounds such as$[(bpmp)Fe_2(O_2CCH_2CH_3)_2][BPh_4]_2$[21] (where $T_2 \approx T_1$), the spectrum was broken into several regions for determination of T_1 values to ensure effective inversion of the spin populations and to avoid having off-axis magnetization when the observe pulse was given.

The intensities of the various peaks as determined by NMCCAP were fit by a nonlinear least-squares program to the equation[22]

$$I(\tau) = I_\infty[1 - (1 + w)\exp(-\tau/T_1)] \quad (1)$$

Three parameters (T_1, I_∞, and w) were allowed to vary. The parameter w generally refined to between 0.70 and 1.00 (the latter value indicates complete population inversion by the 180° pulse).

To ensure accurate integrations for the various paramagnetically shifted resonances, $t_{FID} + t_{delay}$ = 125 ms for Uf_r and 150 ms for Uf_rMoO_4 (~5 × longest T_1). The observed spectrum (without base-line correction) was simulated by a sum of Lorentzian-shaped peaks with the program NMCCAP. To relate the integrations of the peaks to number of protons per protein, an internal standard was used in deuterated buffer. The standard used was 3-(trimethylsilyl)propanoic acid (0.012 M) for Uf_r and acetate (0.1 M) for Uf_rMoO_4. Limitations of instrumental dynamic range and differences in relaxation times required that the spectra of the standard and of the paramagnetically shifted NMR resonances be collected separately in an interleaved fashion. The sharp peaks of the standards were easily resolved from the overlapping broad protein resonances that underlay the sharp peaks.

Results and Discussion

Figures 1 and 2 show the ^1H NMR spectra of reduced uteroferrin and its molybdate and tungstate complexes in the regions outside the normal −1 to 13 ppm range, and Table I summarizes the spectral data. Relatively sharp and well-resolved paramagnetically shifted resonances are observed as expected from the fast electronic relaxation rate of the coupled dinuclear unit.[16]

(16) Lauffer, R. B.; Antanaitis, B. C.; Aisen, P.; Que, L., Jr. *J. Biol. Chem.* **1983**, *258*, 14212–14218.
(17) Keough, D. T.; Dionysius, D. A.; de Jersey, J.; Zerner, B. *Biochem. Biophys. Res. Commun.* **1980**, *94*, 600–605.
(18) Van Geet, A. L. *Anal. Chem.* **1970**, *42*, 679–670. Raiford, D. S., Fisk, C. L., Becker, E. D. *Anal. Chem.* **1979**, *51*, 2050–2051.
(19) Levitt, M. H. *J. Magn. Reson.* **1982**, *50*, 95–110.
(20) Inubushi, T.; Becker, E. D. *J. Magn. Reson.* **1983**, *51*, 128–133.
(21) Borovik, A. S.; Papaefthymiou, V.; Taylor, L. F.; Anderson, O. P.; Que, L., Jr. *J. Am. Chem. Soc.* **1989**, *111*, 6183–6195.
(22) Levy, G.; Peat, I. *J. Magn. Reson.* **1975**, *18*, 500.

Table I. NMR Parameters (300 MHz) for Uf_r, Uf_rMoO_4, and Uf_rWO_4 at 31 °C[a]

peak	δ_{obs}, ppm	$-(d\delta/dT)/(\delta^*/T)$	T_1, ms	fwhh, Hz	$\delta_{J=0}$	r_{eff}
		Uteroferrin (τ_e = 9.1 ps)				
a	86.6	0.88	19.5	1240	104	6.7
b (ex)	88.4		3.8	1180	106	5.1
c	70.0	0.80	7.7	660	84	5.7
d	62.4	0.79	7.3	1170	74	5.7
e (ex)	44				52	
f and g	43.5	0.76	6.8	1020[b]	52	5.6
h	29.5	0.75	5.9	710	35	5.5
i	23.4	0.79	11.3	410	27	6.1
j	15.1	0.34	20.2	180	17	6.8
x (ex)	−24.5	0.96	2.6	1400	−30	4.8
y	−68.0	0.77			−83	
		Uteroferrin–Molybdate (τ_e = 3.4 ps)				
a	103.7	1.37	29.8	380	124	6.4
b (ex)	85.9		9.1	670	103	5.1
c and d	67.7	0.69	12.6	1180	81	5.4
e (ex)	51.5	1.14	13.1	460	61	5.4
f	44.0	0.64	13.7	430	52	5.5
g	43.0		9.6	560	51	5.1
h and i	25.1	0.64	17.2	350	29	5.7
h[c]	25.4		12.9	420	30	5.4
i[c]	25.0		21	240	29	5.9
j[d]	11.6					
k	13.9		29	220	16	6.2
v	−4.6		20	320	−6	5.8
w	−8.4		9	600	−11	5.1
x (ex)	−23.3		6.3	820	−29	4.8
y	−71.6		1	6200	−87	3.5
		Uteroferrin–Tungstate (τ_e = 4.1 ps)				
a	112.7	1.22	27.4	550	135	6.4
b (ex)	88.3	0.71	7.7	820	106	5.1
c and d	72.1		11	1750	86	5.4
e (ex)	54.5	0.93	13.3	730	65	5.6
f	46.4	0.73	16.2	610	55	5.8
g	44.2		11.2	810	52	5.4
h	28.1		13	480	33	5.6
i	23.7	0.78	20.6	320	28	6.0
x (ex)	−23.7		6	1190	−29	4.9
y	−72.0				−88	

[a] All samples were in pH 4.9 buffer containing 0.1 M acetate, and 0.2 M NaCl, and 1–3 mM protein. The quantity $(d\delta/dT)/(\delta^*/T)$ is calculated from spectra taken between 5 and 50 °C, where $\delta^* = \delta_{obs} - \delta_0$. Values of δ_0 used were as follows: b, e: 5 ppm; c, d, and y: 7 ppm; x: 12 ppm; all others: 2 ppm. The full-width at half-height (fwhh) is for H_2O solutions. The right side of the table shows values of δ expected in the absence of coupling (using $\delta^*_{J=0} = \delta^*/0.83$) and r_{eff} relative to the iron(III) site (see text), calculated from the T_1, τ_e, and eq 2 and 3. [b] Overall widths of peaks e–g. [c] Resolved by NMCCAP (Nicolet NT-300) fitting of T_1 inversion–recovery data. [d] Observed in difference spectrum by using saturation transfer from peak a.

The effects of paramagnetic centers on the chemical shifts and relaxation times of nearby nuclei have been covered in detail;[23] the basic theory has also been adapted for molecules with coupled dinuclear paramagnetic metal ions.[24] The contact shift for a particular proton is proportional to the hyperfine splitting constant A_C and the magnetic susceptibility of the complex. A_C values for protons on nonbridging amino acids of uteroferrin are expected to be similar to those found in appropriate mononuclear model complexes, but the magnetic susceptibility of the metal center in the direction of the applied field, i.e., $\langle S_z \rangle / H_0$, will be reduced by the weak antiferromagnetic coupling. Using parameters from the fit of the magnetic susceptibility data ($2J = -19.8$ cm^{-1}),[11] we calculate that at room temperature contact shifts for uteroferrin will be reduced by ca. 17% from those predicted for mononuclear complexes with $g = 2.0$.[25,26] Thus, for proper comparison with values from mononuclear model complexes, δ_{obs} values must be scaled up to $\delta_{J=0}$ values.

The dipolar contributions to the isotropic shift can be calculated from the expected magnetic anisotropy.[25] Based on these calculations, a proton 5 Å from the metal center could experience δ_{dip} between −17 and +13 ppm for Fe(II) but $\leq \pm 2$ for Fe(III). These calculated dipolar shifts are considerably less than most of the observed isotropic shifts, confirming the predominance of the contact interactions for most of the observed Uf_r resonances.

Paramagnetic Shift Changes Upon Anion Binding. Uf_r binds a variety of tetraoxoanions. Only small changes are observed when molybdate or tungstate are added to Uf_r. The observed shifts are summarized in Table I and illustrated in Figures 1 and 2. Peaks have been identified by letters in these figures, and peaks assigned the same letter in different complexes are assumed to correspond to the same protons based on similarities in chemical shift, relaxation properties (see below), and solvent exchangeability. Each letter corresponds to one proton per protein molecule (determined by peak intensity integrations as described below), except for y, the broadness of which renders accurate integration difficult. In each spectrum there is partial or complete overlap (or degeneracy) of several resonances. For instance, in Uf_r, D_2O-exchangeable resonance e and nonexchangeable resonances f and g are superimposed at δ = 44 ppm. In some cases, the resonance positions of the observed peaks have been resolved by peak fitting.

A titration of molybdate into a sample of uteroferrin revealed that, for less than one equivalent of molybdate added, NMR resonances corresponding to both Uf_r and Uf_rMoO_4 are observed, and that NMR spectral changes are complete when 1.0 equiv of molybdate is added, although cloudiness (protein denaturation) was noticed when >1.2 equiv of molybdate was added.[14] This indicates that exchange rate for oxoanion binding is slow on the NMR time scale, so that the spectra shown in Figures 1 and 2 are of discrete molecular species.

The spectrum obtained by adding arsenate to an anaerobic sample of Uf_r at pH 4.9 (Table II) is very similar to those of Uf_r, Uf_rMoO_4, and Uf_rWO_4. The exclusion of oxygen is necessary because arsenate, like phosphate, promotes the air oxidation of the dinuclear site to the diferric oxidation state.[14] We have been unable to observe NMR resonances associated with any form of

Table II. Observed Chemical Shifts at 40 °C for Uteroferrin Complexes

peak	chemical shifts, δ (ppm) Uf_rAsO_4 (pH 4.9)[a]	Uf_r (pH 3)[b]	Uf_rPO_4 (pH 3)[c]
a	89.9	82	142
b (ex)	86.7	87	100
c and d	63.6	64	100
e (ex)	49.9	43	55
f	47.2	42	50
g	39.6	42	40
h	27.3	23	32
i	24.9	23	26
j			20
x (ex)	−21.5	−19	−19
y			−115

[a] In 0.1 M sodium acetate buffer, pH 4.9 [b] In 0.1 M sodium citrate buffer, pH 3. [c] In 0.1 M sodium citrate buffer, pH 3, and 0.1 M NaH_2PO_4.

(23) (a) Bertini, I.; Luchinat, C. *NMR of Paramagnetic Molecules in Biological Systems*; Benjamin/Cummings: Menlo Park, CA, 1986. (b) LaMar, G. N.; Horrocks, W. D., Jr.; Holm, R. H. *NMR of Paramagnetic Molecules. Principles and Applications*; Academic: New York, 1973.

(24) Owens, C.; Drago, R. S.; Bertini, I.; Luchinat, C.; Banci, L. *J. Am. Chem. Soc.* **1986**, *108*, 3298–3303. Equations A1 and A2 should have a division sign before the last term and eq A3 requires summation over all multiplets.

(25) Calculations of $\langle S_{iz} \rangle$, $\langle S_i^2 \rangle$, and magnetic anisotropy used the Hamiltonian

$$\mathcal{H} = -2J S_2 \cdot S_3 + \sum_{i=2}^{3} (D_i(S_{iz}^2 - S_i^2/3) + E_i(S_{ix}^2 - S_{iy}^2) + \mu_B \mathbf{S}_i \mathbf{g}_i H_0)$$

with the 30-state basis set of $S_2 = 2$ and $S_3 = {}^5/_2$. The subscript i denotes the valence of the iron atom. The parameters were obtained from a fitting of the magnetic susceptibility and EPR spectra of reduced uteroferrin.[1]

(26) Although antiferromagnetic coupling reduces the magnitude of $\{S_z\}$ proportionately more for Fe(II), this decrease is offset by the larger zero-field splitting ($g_{eff} > 2$) of the Fe(II).

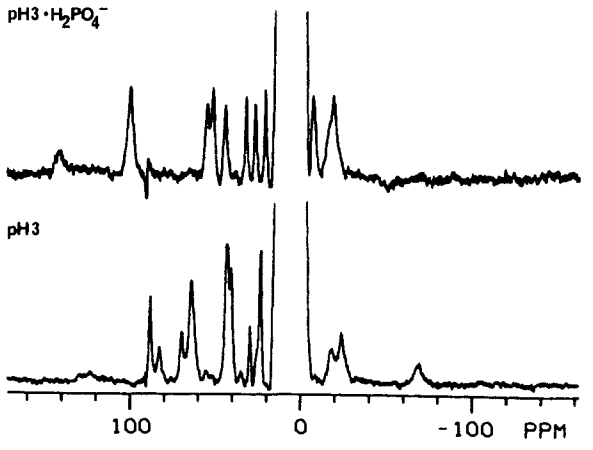

Figure 3. Base-line-corrected 300-MHz ^{1}H NMR spectra at 40 °C of pH 3.0 solutions of (a) (upper) $UfPO_4$ prepared anaerobically to prevent oxidation and (b) (lower) Uf_r.

oxidized uteroferrin; this is presumably due to the stronger antiferromagnetic coupling[6,16] (smaller shifts) and/or the slower electronic relaxation rate (broader peaks) of the Fe(III)–Fe(III) cluster.[23]

When phosphate (20 mM or greater) is added to reduced uteroferrin at pH 4.9 under anaerobic conditions, the resulting solution exhibits no readily identifiable paramagnetically shifted NMR resonances.[27] We have confirmed this result, which is particularly surprising given our results with arsenate. However, at pH 3, under anaerobic conditions, we are able to observe an NMR spectrum of the reduced uteroferrin phosphate complex (Figure 3a and Table II), which exhibits isotropic shifts greater than those for Uf_r and the other anion complexes. Unfortunately, the protein denatures over several hours under these conditions, resulting in loss of all observable paramagnetically shifted NMR resonances.

The spectrum of anion-free Uf_r at pH 3 (Figure 3b) shows peaks in addition to those observed at pH 4.9. The spectrum at pH 3 is interpretable as a superposition of two states of the protein—namely, the same form as observed at pH 4.9 and a low-pH form, whose NMR shifts are given in Table II. The observation of separate NMR peaks for the low- and high-pH forms of Uf_r indicates that a relatively slow conformational change is coupled with the protonation of the protein. Such pH-dependent effects have also been observed in the EPR spectra of the enzyme from bovine spleen.[6] The apparent NMR silence of Uf_rPO_4 at pH 4.9 could be due to the existence of multiple forms of the protein, which give rise to severely overlapping peaks.

The protons giving rise to the paramagnetically shifted NMR resonances are almost certainly the same protons that give rise to the seven hyperfine couplings observed in the ENDOR spectra of Uf_r and Uf_rMoO_4. Two of these couplings are of D_2O-exchangeable protons.[28] The couplings observed by ENDOR at 2 K range from 1 to 5 MHz; these are larger in magnitude than those we observed by NMR because no orientational or excited electronic state averaging of dipolar shifts occurs in ENDOR.

Temperature Dependence of Various Resonances. The temperature dependence of the various paramagnetically shifted NMR resonances of Uf_r has been described and was used to obtain an estimate of $2J = -20$ cm^{-1} for the antiferromagnetic coupling between the Fe(II) and Fe(III) sites of the dinuclear center,[16,29] a result that has since been confirmed by a magnetic susceptibility study.[11] Tabulated in Table I are $-[(d\delta/dT)/(\delta^*/T)]$ values for the paramagnetically shifted resonances, which correspond to the decreases in chemical shift with increasing temperature relative to Curie law behavior, i.e., no coupling. Assuming contact shifts to be dominant, $-[(d\delta/dT)/(\delta^*/T)]$ is predicted to be 0.67 for ligands of the iron(II) or 0.77 for ligands of the iron(III) on the dinuclear center of Uf_r.[25] Where the temperature dependence of δ could be measured with confidence (overlapping peaks in some cases prevented this), we find $-[(d\delta/dT)/(\delta^*/T)]$ between 0.64 and 0.8 for peaks b–d, f, h, i, and y in Uf_r, Uf_rMoO_4, and Uf_rWO_4. This and the very similar δ values for these peaks indicate that the $2J$ value of -20 cm^{-1} is virtually unchanged upon molybdate or tungstate binding. Peaks a, e, and x have greater values of $-[(d\delta/dT)/(\delta^*/T)]$, which can indicate either significant dipolar contributions to δ^* (dipolar shifts can decrease with temperature more rapidly than contact shifts) or that A_C is temperature dependent (as will be seen, this latter explanation is likely for peak a).

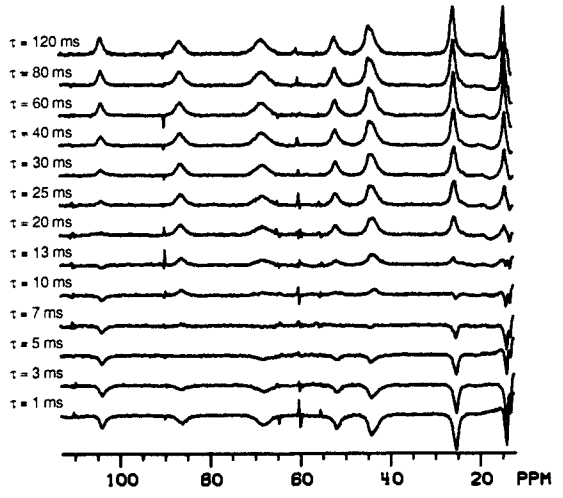

Figure 4. Base-line-corrected 300-MHz ^{1}H NMR spectra from T_1 inversion–recovery experiment on Uf_rMoO_4 at 31 °C, pH 4.9. For this experiment, $t_{FID} = 20$ ms (4K points in FID), $t_{delay} = 105$ ms, and each spectrum is from the sum of 16 000 FIDs, collected in batches of 2000. All spectra are phased identically. Peak intensities were determined prior to cubic spline base-line correction by using the spectral simulation program NMCCAP to fit the height, width, and δ of the peaks. The width and δ of each peak were held to the same values for each of the 13 spectra; this allows the determination of separate δ, widths, and intensities for overlapping peaks f/g and h/i. For instance, comparison of spectra with $\tau = 5$ and 13 ms shows changes in δ and width for the ca. 44 ppm peak, which are interpreted as the predominance of peaks f and g, respectively, in these two spectra.

The shifts observed for Uf_rPO_4 at pH 3 are greater in magnitude and exhibit a temperature dependence more closely approximating Curie behavior with $-[(d\delta/dT)/(\delta^*/T)]$ values of 1.12, 0.95, and 1.15 for peaks c/d, g, and h, respectively, suggesting that the antiferromagnetic coupling interaction is absent or substantially weaker in this complex. This weakening of the antiferromagnetic coupling has also been observed in magnetic susceptibility studies of Uf_rPO_4 at pH 4.9 ($2J = -6$ cm^{-1}).[11]

Integrations. The concentration of the Uf_r sample used for NMR peak integrations was 1.0 mM using $\epsilon_{vis} = 4000$ M^{-1} cm^{-1}, but the slight red shift in the λ_{max} to 516 nm indicated that some of the protein had oxidized. Quantitation of the EPR signal of the same sample showed a spin concentration of 0.8 mM. The NMR integrations, obtained by curve fitting and normalized to 0.8 mM protein, were 1.1, 1.3, 1.2, 2.0, 1.0, and 1.1 for peaks a, c, d, f/g, h, and i, respectively. The $UfMoO_4$ was 1.1 mM by its visible spectrum, and its NMR integrations give 0.8, 1.7, 1.8, and 1.9 protons/protein for peaks a, c/d, f/g, and h/i. These results indicate that each lettered peak in the downfield region corresponds to one proton per uteroferrin molecule. Integrations of peaks obtained in H_2O buffer indicate that peaks b, e, and x also correspond to one proton per protein. Because of its width, peak y could not be reproducibly fit.

(27) Doi, K.; Gupta, R.; Aisen, P. *J. Biol. Chem.* **1987**, *262*, 6982–6985.
(28) Doi, K.; McCracken, J.; Peisach, J.; Aisen, P. *J. Biol Chem.* **1988**, *263*, 5757–5763.
(29) The model used to fit the temperature-dependence data in ref 16 incorrectly assumed that the valences were delocalized. However, use of the valence-localized model subsequently described in ref 30 did not significantly alter the estimate for J, a value confirmed but more precisely determined by magnetic susceptibility measurements.[11]
(30) Maroney, M. J.; Kurtz, D. M., Jr.; Nocek, J. M.; Pearce, L. L.; Que, L., Jr. *J. Am. Chem. Soc.* **1987**, *108*, 6871–6879.

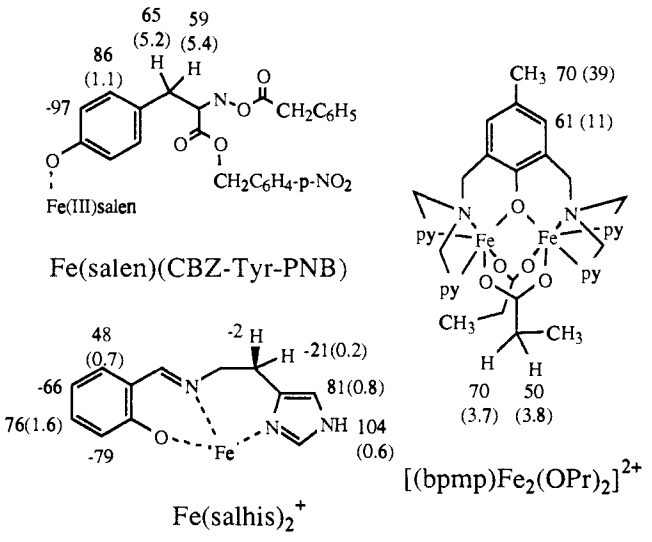

Figure 5. Chemical shift and relaxation data for protons of several iron complexes containing features of amino acid side chains. δ_{obs} is shown along with the T_1 values in milliseconds in parentheses.

T_1 Relaxation Measurements. Data from a typical inversion–recovery experiment are shown in Figure 4. The increase in peak intensity with increasing delay time τ was fit to eq 1 to give T_1 values for the various resonances, as shown in Figure S1 (supplementary material) and tabulated for Uf_r, Uf_rMoO_4, and Uf_rWO_4 in Table II. In addition to providing T_1 values of the various resonances, the inversion–recovery data allowed us to obtain more accurate chemical shift and line-width information for overlapping peaks. For instance, the τ = 5 ms spectrum of Figure 4 shows a negative peak at 44 ppm, while the τ = 10 ms spectrum shows a small positive peak at 43 ppm. This results from the faster relaxation of peak g (43 ppm) compared with peak f (44 ppm). In fitting this region of the spectrum of Lorentzian peaks, the peak positions were determined from the τ = 5 and 10 ms spectra and the widths adjusted to give equal integrations for f and g at τ = 120 ms. Then heights were fit to the two peaks for each of the 13 spectra. A similar procedure was used to deconvolute peaks h and i, which are separated by only 0.4 ppm, but which have significantly different widths. The exponential fits to the deconvoluted peak intensities were nearly as good as the fits to peak heights for isolated peaks (see Figure S1).

The T_1 values observed for Uf and its anion complexes are due primarily to dipolar relaxation. We have thus adapted the dipolar relaxation equation to reflect the presence of a coupled dinuclear $Fe^{II}Fe^{III}$ unit as follows:

$$T_1^{-1} = f(\tau_e,\omega_s)(g_3^2\langle S'^2_3\rangle)r_{eff}^{-6} \quad (2)$$

where $f(\tau_e,\omega_s)$ is a collection of terms from the Solomon–Bloembergen equation, which can be considered a constant for a given protein at a given magnetic field. The subscript 3 in the $g_3^2\langle S'^2_3\rangle$ term denotes the Fe(III) ion, and the prime denotes the component of S_a parallel to the overall spin of the antiferromagnetically coupled system. The value for r_{eff} is calculated by adding the effects of relaxation by the Fe(III) (denoted by subscript 3) and the Fe(II) ions (denoted by subscript 2) together with the effects of ligand-centered dipolar relaxation:[23a]

$$r_{eff}^{-1} = \left[\frac{1}{r_{3H}^6} + \frac{\rho_\pi^2}{r_{\pi H}^6} + \frac{g_2^2\langle S'^2_2\rangle}{g_3^2\langle S'^2_3\rangle r_{2H}^6}\right]^{1/6} \quad (3)$$

In this equation, ρ_π is estimated from the A_C value by using the McConnell equation and refers to the spin density on the ligand carbon atom as a fraction of the total (multielectron) spin.[23] (This differs from ρ_C^π of eq 2.14 in ref 23a, which represents a fraction of a single unpaired electron.)

Thus, a linear relation between T_1 and r_{MH}^6, where r_{MH} is the shorter M–H distance in the complex, is not expected because of the presence of two paramagnetic ions at the metal site of Uf_r

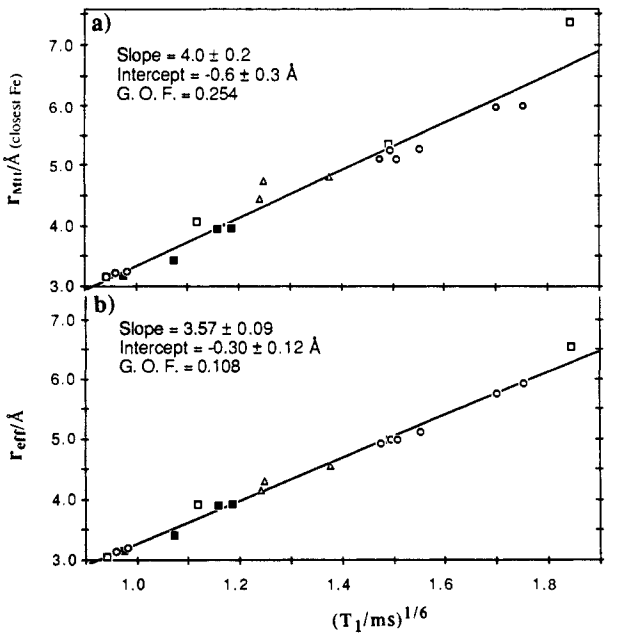

Figure 6. Plots of (a) r_{MH} and (b) r_{eff} calculated from coordinates of the crystal structure vs measured $T_1^{1/6}$ for $[(bpmp)Fe_2(OPr)_2][BPh_4]_2$. Symbols indicate assignments for various resonances, with δ in ppm as follows (listed from low to high T_1): □, mesitylene CH_2 (103, 377) μ-(61) and p-CH_3 (70); ■, pyridylmethyl CH_2 (40, 14, 253, 177); ○, pyridyl 6-H (191, 158), 3,5-H (77, 53, 65, 71), and 4-H (4, 5); △, propionate CH_2 (70, 50) and CH_3 (18). NMR spectra were measured at 25° C in acetone-d_6.

and because of the effects of ligand-centered dipolar relaxation. To confirm the applicability of eq 2 and 3, we have applied them to T_1 data obtained for the protons of $[(bpmp)Fe_2(OPr)_2]^{2+}$ (see Figure 5). Crystal structures are available for both this mixed-valence $Fe^{II}Fe^{III}$ complex and the analogous $Zn^{II}Fe^{III}$ complex;[21] average distances from the two structures are used to estimate r_{3H} and r_{2H} for eq 3. Although the crystal structure and low-temperature Mössbauer spectrum of this complex show localized iron(II) and iron(III) sites (both high spin), the intervalence charge transfer is rapid enough at room temperature that ligands bound to both iron atoms are equivalent by NMR; the assignments of peaks are described elsewhere.[21] Thus, for this complex, we use $g_3^2\langle S'^2_3\rangle = g_2^2\langle S'^2_2\rangle$ in eq 3.

Figure 6 shows plots of r_{MH} (closest Fe–H distance from crystal structures) and r_{eff} (from eq 3) vs $T_1^{1/6}$. It is evident that $T_1^{1/6}$ is more nearly proportional to r_{eff} than to r_{MH}; this is particularly apparent for protons on the bridging propionate and phenolate groups. The goodness of fit (gof = $[\sum(r_{line} - r)^2/(n_{data} - 2)]^{1/2}$) of the best fit line decreases from 0.24 to 0.11 when r_{eff} is used instead of r_{MH}. Ligand-centered relaxation is relatively unimportant, accounting on the average for only one-sixth of the reduction of r_{eff} from r_{MH}. Inclusion or exclusion of the ρ_π^2/r_π^6 term in the calculation of r_{eff} made less than 1% difference in the gof value of the straight-line fit of r_{eff} vs $T_1^{1/6}$. Note that the intercept of the best fit line of Figure 6b is less than zero by 2.5 standard deviations. This is probably due to the use of the point dipole approximation for the metal ions; we obtain an intercept of –0.4 ± 0.1 Å by plotting theoretical $T_{1M}^{1/6}$ values vs r calculated by use of solid spherical harmonics to represent spin density of $S = {}^1/_2Fe^{3+}$.[31] The effect of the spatial extent of the spin density on the iron atoms (which is not accounted for by eq 3 becomes less important for protons with $r_{MH} > 4$ Å[32] and thus has been neglected in the analysis of Uf_r T_1 values.

In order to use the protein T_1 data for peak assignments, it was necessary to estimate r_{eff} values for various possible ligating groups.

(31) Gottlieb, H. P. W.; Barfield, M.; Doddrell, D. M. *J. Chem. Phys.* **1977**, *67*, 3785–3794.

(32) Doddrell, D. M.; Healy, P. C.; Bendall, M. R. *J. Magn. Reson.* **1978**, *29*, 163–166.

Table III. Chemical Shifts and Actual and Effective Iron–Proton Distances (r_{MH} and r_{eff}) Expected for Protons of Likely Amino Acid Ligands to the Dinuclear Site in Uteroferrin[a]

	δ_0	$\delta(Fe^{2+})$	$\delta(Fe^{3+})$	r_{MH}(est)	$r_{eff}(Fe^{2+})$	$r_{eff}(Fe^{3+})$
histidine[16,38]						
NH	5	57 to 68	97 to 104	5.1–5.4	5.2–5.9	4.9–5.3
$C_\delta H$ (N_δ)	7	47 to 63	78 to 82	5.1–5.4	5.2–5.9	4.9–5.3
β-CH_2 (N_ϵ)	2	$7 f(\theta_H)^b$	$19 f(\theta_H)^b$	5.5–6.5	5.6–7.1	5.3–6.4
β-CH_2 (N_δ)	2			3.0–4.7	3.3–5.2	3.0–4.7
tyrosine[14,16,37]						
o-H	7	−15	−101 to −94	3.1–4.4	3.4–4.9	3.1–4.4
m-H	7	11	85 to 89	5.4–6.3	5.5–6.7	5.2–6.0
β-CH_2	2	$20 f(\theta_H)^b$	$110 f(\theta_H)^b$	7.0–7.7	6.9–8.3	6.7–7.5
Asp-β-(Glu-γ)-CH_2[21,36]						
terminal	2	$30 f(\theta_H)^{b,c}$	$(25–125) f(\theta_H)^b$	4.2–5.1	4.4–5.7	4.1–5.1
O,O′-bridging	2	$60 f(\theta_H)^{b,d}$		4.3–5.0	4.0–4.7	

[a] Values of δ are based on model complexes, and r_{eff} depends on which iron (Fe^{2+} or Fe^{3+}) the ligand binds. The values of r_{MH} were estimated in part by using crystal structures of model complexes, but largely through the use of the program MOLECULAR EDITOR[33] to investigate the effects of possible conformational changes. [b] Methylene protons modeled by methyl groups. The scalar value represents the shift observed for a methyl group in that position; this value should be scaled by $f(\theta_H) \approx 2\cos^2\theta_H$ to take into account the dependence of isotropic shifts on the torsion angle θ_H. The shift of a methylene proton is expected to equal that of the methyl when $\theta_H = 45°$ (cf. eq 4; in other conformations, $f(\theta_H)$ ranges from 0 to 2. [c] This value is based on the acetate CH_3 shift of $[Fe^{II}Zn^{II}(bpmp)(OAc)_2]BPh_4$ prepared by T. R. Holman. [d] The value shown is based on the observed CH_2 shifts of the mixed-valence model complex $[(bpmp)Fe_2(OPr)_2]^{2+}$, which was prepared by A. S. Borovik and has a value of $-2J < 10$ cm^{-1}.

Table III shows values of r_{MH} estimated from molecular modeling[33] (and crystal structures, where known). The distance to the further iron is estimated from r_{MH}, $r_{Fe-Fe} = 3.1$ Å,[34,35] and the assumption that $90° < \angle Fe_{far}–Fe_{close}–H < 180°$ for nonbridging ligand. For a bridging ligand we assume $r_{3H} = r_{2H} = r_{MH}$, and eq 3 is used to calculate r_{eff}. The values of r_{eff} are ~5% less than r_{MH} for ligands bound to Fe^{3+}, while r_{eff} is ~5% greater than r_{MH} for ligands bound only to Fe^{2+}.

Peak Assignments. We have assigned several of the NMR peaks of uteroferrin on the basis of observed chemical shifts, the presence or absence of the peaks in D_2O or at high pH, distance estimates based on the T_1 values, and, in one case, on the observation of cross relaxation (nuclear Overhauser effect) between peaks. Our assignments are aided by the assignment of resonances in iron complexes having ligand containing phenolate,[16,37] imidazole,[16,38] and carboxylate[21,36] ligands resembling those that occur in proteins. Examples of such complexes are shown in Figure 5. Table III indicates ranges of chemical shifts observed in various model complexes, which can be compared with $\delta_{J=0}$ shown in Table I.

It is evident that most of the observed NMR resonances of Table I could be assigned to several of the possible ligands listed in Table III. However, the loss of resonances b, e, and x when deuterated buffer is employed indicates that these protons exchange with water. Of the amino acid side chains that commonly coordinate iron in metalloproteins, only histidine possesses such exchangeable protons. On the basis of comparisons with model complexes (Table III), resonances b and e are assigned to the NH protons of one histidine coordinated to iron(III) and one histidine coordinated to iron(II), respectively. The spectrum of Uf_r is remarkably pH independent between pH 4.9 and 9.5. The only change involves peak b, which at pH 8.5 is significantly broader than at pH 4.9, and at pH 9.5 is not observed (data not shown). This suggests that at pH 9.5, the NH group responsible for peak b has either deprotonated or is in rapid exchange with solvent water. The latter possibility is more likely since the other peaks do not shift as the pH is increased to 9.5. The behavior of peak b supports its assignment to a histidine ligand. Histidine bound to cobalt(II) in cobalt-substituted liver alcohol dehydrogenase has been shown by NMR to deprotonate with a pK_a of ~9.[39]

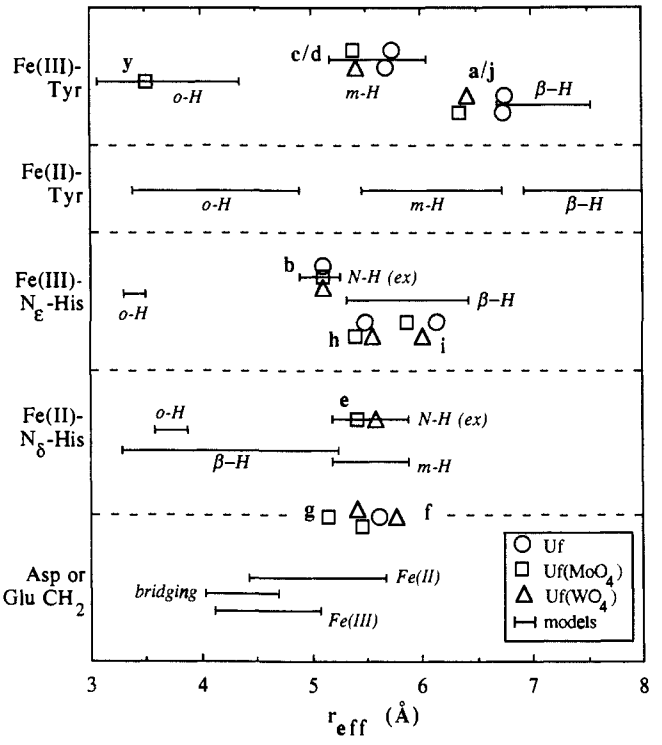

Figure 7. Plot showing r_{eff} for various lettered resonances from Table I along with ranges of r_{eff} values expected for various possible ligating groups (cf. Table III). The resonances and ligand types follow (from top to bottom) the order of discussion in the text.

We have used peak b [NH on His-Fe(III)] to determine τ_e for Uf_r, Uf_rMoO_4, and Uf_rWO_4 by selecting the value of the electronic relaxation τ_e that gives for peak b $r_{eff} = 5.1$ Å, the middle of the 4.9–5.3 Å range expected. The uncertainties in r_{eff} affect τ_e, but it is clear that the electronic relaxation is roughly twice as fast for Uf_rMoO_4 and Uf_rWO_4 as for anion-free Uf_r (Table I). The r_{eff} for other resonances can be calculated by using τ_e and measured T_1 values, as listed in Table I and shown graphically in Figure 7. Because of the uncertainty in the true value of r_{eff} for peak b, the calculated r_{eff} values in Table I and Figure 7 have an uncertainty of ca. ±4%.

The r_{eff} and $\delta_{J=0}$ values calculated for exchangeable peak e in Uf_rMoO_4 and Uf_rWO_4 are exactly in the center of the range

(33) Wargo, R.; Smith, A.; McFerren, D. *"Molecular Editor" for the Macintosh computer*, Drexel University, 1986. Available through Kinko's Academic Courseware Exchange.
(34) Que, L., Jr.; Scarrow, R. In *Metal Clusters in Proteins*; Que, L., Jr., Ed.; ACS Symposium Ser. 372; American Chemical Society: Washington DC, 1988; pp 152–178.
(35) Kauzlarich, S. M.; Teo, B. K.; Zirino, T.; Burman, S.; Davis, J. C.; Averill, B. A. *Inorg. Chem.* **1986**, *25*, 2781–2785.
(36) Arafa, I. M.; Goff, H. M.; David, S. S.; Murch, B. P.; Que, L., Jr. *Inorg. Chem.* **1987**, *26*, 2779–2784.
(37) Mukherjee, R. N.; Abrahamson, A. J.; Patterson, G. S.; Stack, T. D. P.; Holm, R. H. *Inorg. Chem.* **1988**, *27*, 2137–2144.
(38) Wu, F.-J.; Kurtz, D. M., Jr. *J. Am. Chem. Soc.* **1989**, *111*, 6563–6572.
(39) Bertini, I.; Gerber, M.; Lanini, G.; Luchinat, C.; Maret, W.; Rawer, S.; Zeppezauer, M. *J. Am. Chem. Soc.* **1984**, *106*, 1826–1830.

predicted for histidine bound to iron(II) (Figure 7). Thus, the exchangeability, chemical shifts, and relaxation times all support the assignments of peaks b and e to protons of histidine ligands to Fe(III) and Fe(II), respectively. The integrations of these peaks indicate that each iron is bound by only one NMR-detectable histidine.

Once τ_e is calculated, it is possible to verify the assumption inherent in these calculations that dipolar relaxation is virtually the sole determinant of T_1 values. Calculations for peaks b and e indicate that the percentage of relaxation caused by various mechanisms is as follows: dipolar by Fe(III), 81% (b) and 24% (e); dipolar by Fe(II), 6% and 69%; ligand-centered dipolar, 10% and 5%; Curie and contact, ≤2% for both b and e.

Resonance Raman studies unequivocally demonstrate the presence of tyrosinate ligation to the Fe(III) of the cluster.[12] Ortho protons of such a tyrosine are expected to exhibit large upfield shifts. Thus, peak y (at −70 ppm) is assigned to one or two ortho protons of a tyrosine ligand to Fe(III). In addition to the ortho protons, meta and β-CH_2 protons of the tyrosine should be observed in the NMR spectrum. On the basis of NMR spectra of complexes between tyrosine derivatives and $[Fe(salen)]^+$ (cf. Table III and Figure 5), resonances between 62 and 72 ppm are assigned to meta protons. In Uf_r, peaks are observed at both 62 and 70 ppm. The presence of two peaks is ascribed to slow rotation (τ_{rot} > 0.3 ms) of the tyrosine about the C_β–C_γ bond; at 50 °C the peaks begin to coalesce.[16] The difference in chemical shifts between the two meta protons is probably due to dipolar effects, including those of the distant, but more anisotropic Fe(II). In the anion complexes of uteroferrin, a single peak (integrating to two protons) is observed in the 64–72 ppm region, indicating that in these molecules tyrosine rotation is faster or that the intrinsic difference in chemical shift between the two meta protons is less due to changes in the spin anisotropy of the dinuclear iron center.

The r_{eff} values calculated for peaks c and d lie between 5.4 and 5.7 Å, centered within the range expected for meta protons on tyrosine. Also, r_{eff} = 3.5 Å for peak y in Uf_rMoO_4, reasonable for an ortho tyrosine proton. These fits add confidence to our determination of τ_e based on peak b.

Our previous assignment of the nonexchangeable peaks f and g to the β-CH_2 protons of tyrosine was based on the close correspondence of the $\delta_{J=0}$ with the $\delta(CH_2)$ found in model ferric–tyrosinate complexes.[16] However, this assignment is inconsistent with the T_1 relaxation data, as r_{eff} values of 5.1–5.8 Å are observed (Table I), whereas a value of at least 6.7 Å is expected (Table III and Figure 7).[40] We also note that the ratio of T_1 values (p-CH_n/meta) for model complexes Fe(salen)(CBZ-Tyr-PNB)$^+$ and $[(bpmp)Fe_2(OPr)_2][BPh_4]_2$ are 4.8 and 3.5, respectively, while the average ratio ({c,d}/{f,g}) for the uteroferrin samples is 1.0. Thus, the β-methylene protons of the coordinated tyrosine in uteroferrin must give rise to peaks other than f and g in the NMR spectra.

The only peaks outside the diamagnetic NMR manifold having T_1 values consistent with $r_{eff} \geq 6.7$ Å are peaks a and j of Uf_r.[40] For Uf_rMoO_4 and Uf_rWO_4 the longest calculated r_{eff} is 6.4 Å [with estimated uncertainty (see above) of 4% = ±0.25 Å], so a is the best candidate for one of the tyrosine β-CH_2 peaks. Peak j is observed at the edge of the diamagnetic manifold and so was initially considered an unlikely candidate for a tyrosine CH_2 proton. However, peak a integrates to only one proton per protein,

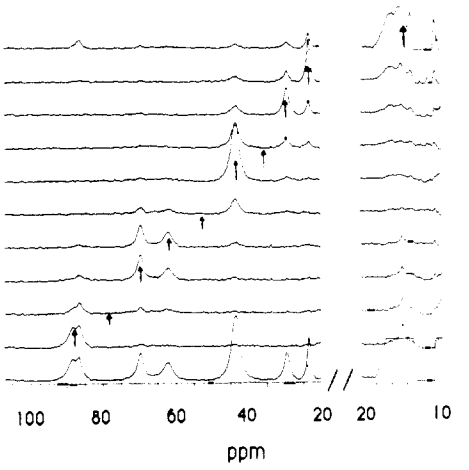

Figure 8. Nuclear Overhauser effect observed between peaks a and j of Uf_r by decoupler irradiation during the last 80 ms of the 95 ms τ of super-WEFT pulse sequence ($t_{FID} + t_{delay}$ = 125 ms). The spectrum at the bottom is the control with the decoupler at 150 ppm. For other spectra, the arrows show the position of the decoupler frequency, and the difference spectrum (control − decoupler, at arrow) is shown. The relatively short periods of decoupler irradiation result in off-resonance peak suppression.

Table IV. Calculations of Torsion Angle θ_α(C_α–C_β–C_γ–[π orbital on C_γ] for Coordinated Tyrosine in Uteroferrin and Model Ferric–Tyrosinate Complexes from NMR shifts

	δ_{meta}, ppm	$\delta_{\beta1}$, ppm	$\delta_{\beta2}$, ppm	$\lvert\theta_\alpha\rvert_{av}$, deg	σ_θ, deg
Fe(salen)(NAc-Tyr-OMe)	85	61	58	0.5	14.2
Fe(salen)(CBZ-Tyr-PNB)	86	65	59	1.1	16.3
Fe(salen)(Tyr-OMe)	87	73	53	3.7	16.2
Uf_r(pH 4.9)	66	87	15	17.6	11.7
Uf_r(pH 3)	64	82	(12)[a]	16.9	12.0[a]
Uf_rPO_4 (pH 3)	100	142	20	19.5	12.0
Uf_rAsO_4	64	90	(12)[a]	20.6	12.0[a]
Uf_rMoO_4	68	104	12[b]	23.8	12.8
Uf_rWO_4	72	113	(11)[a]	24.3	12.0[a]

[a] $\delta_{\beta2}$ was not observed, but was calculated by using σ_θ = 12°. [b] $\delta_{\beta2}$ observed in NOE experiment with irradiation at $\delta_{\beta1}$.

so the other tyrosine methylene proton must give rise to peak j (in Uf_r) or lie under the diamagnetic protein signal. Figure 8 shows difference NMR spectra obtained by irradiation of selected peaks during time τ of the super-WEFT pulse sequence. This revealed saturation transfer from peak a to peak j (15 ppm) in Uf_r. A similar experiment (not shown) showed saturation transfer from peak a to a peak at 11.4 ppm [visible only in the difference (normal − irradiated) spectrum] in Uf_rMoO_4; saturation transfer was also observed to peak a in both Uf_r[42] (Figure 8) and Uf_rMoO_4 as a result of irradiation in the 11–15 ppm region. Similar magnetization transfers due to the nuclear Overhauser effect have been observed in paramagnetic heme proteins.[43]

But why do the tyrosine β-CH_2 protons resonate at $\delta \geq 86$ ppm and $\delta \leq 15$ ppm when model ferric–tyrosinate complexes would predict δ between 40 and 60 ppm? Ferric–tyrosinate complexes show considerably more variability in their β-CH_2 shifts than in the shifts of the ring protons (Table IV). This variability is due to the proportionally of the shifts of the methylene protons to $\cos^2 \theta_H$, where θ_H is the torsion angle involving H_β–C_β–C_γ–(π orbital on C_γ):[44]

$$\delta_{con} = k\rho_\pi(\cos^2 \theta_H) \quad (4)$$

(40) The minimal r_{eff} of 6.7 Å shown in Table V was found by using an $\angle$Fe–O–C_{tyr} of 120° (the shortest deemed reasonable; this angle lies between 130 and 140° in crystallographically characterized iron phenolates[41]) and assuming $\angle Fe^{2+}$–Fe^{3+}–$H_{methylene}$ = 90°. Shorter values of r_{eff} can be calculated by assuming a conformation where $\angle Fe^{2+}$–Fe^{3+}–$H_{methylene}$ < 90°; specifically a conformation where a nonbridging tyrosine is coordinated cis to both bridging ligands in a doubly bridged dimer, and the Fe–O–C_{tyr} angle is arranged so that the phenyl ring is angled toward the iron(II). The shortest r_{eff} possible from an extreme conformation of this type is 6.1 Å, but the values of r_{eff} for the meta protons also decrease to ~5.0 Å, which is shorter than that observed for peaks c and d. Thus, peak i cannot be a tyrosine methylene, although a slight angling of the phenyl toward the iron(II) may explain the r_{eff} of <6.7 Å observed for $UfMoO_4$ and $UfWO_4$.

(41) Heistand, R. H., II; Roe, A. L.; Que, L., Jr. *Inorg. Chem.* **1982**, *21*, 676.

(42) The saturation transfer difference spectrum of Uf irradiated at 14 ppm (Figure 8) shows a peak at 86 ppm—clearly to peak a and not to peak b (at 88 ppm). The observed NOE (η) on peak a upon irradiation of peak j is −0.3. The cross-relaxation rate $\sigma_{aj} \approx \eta(T_1^{-1})_a \approx 15\ s^{-1}$ can be related to the interproton distance r_{aj} and τ_{rot} by $\sigma_{ij} = -0.109(h/2\pi)^2\gamma^4 r_{aj}^{-6}\tau_{rot}$. Assuming r_{aj} = 1.77 Å, one can calculate τ_{rot} = 8 ns, close to the value of 11 ns estimated from the Stokes–Einstein equation.[23]

(43) Thanabal, V.; de Ropp, J. S.; La Mar, G. N. *J. Am. Chem. Soc.* **1987**, *109*, 265–272, and references therein.

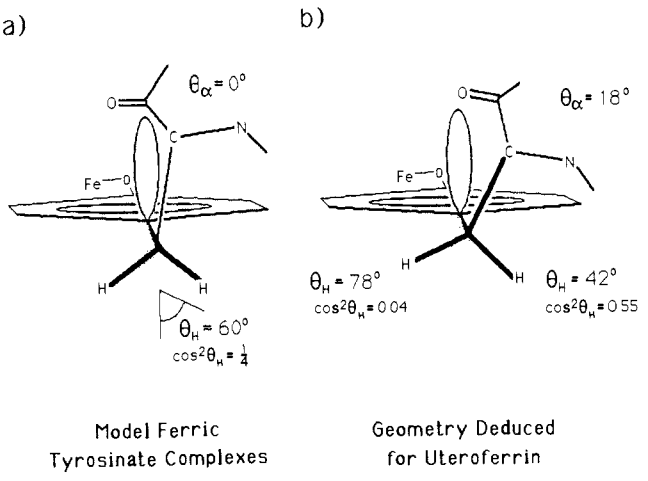

Figure 9. Geometry of tyrosine in (a) Fe(salen)(tyrosinate) model complexes and (b) uteroferrin deduced from NMR shifts (cf. eq 4 and Table IV).

ρ_π can be estimated from the shift of the meta proton, which is proportional to the delocalized spin on the π system. The proportionality constant k can be determined from the methyl shift of the complex (p-$CH_3C_6H_4O$)Fe(salen), where $\langle\cos^2\theta_H\rangle$ averages 0.5 because of the free rotation of the methyl group. Assuming the same k, we can use the NMR spectra of the coordinated tyrosine in uteroferrin and model complexes to determine the torsion angles $\theta_H = \theta_\alpha \pm 60°$, where θ_α is the torsion angle of η_α–C_β–C_γ–(π orbital on C_γ) (see Figure 9). We include the degree of torsional motion σ_θ in the calculation of $\langle\cos^2\theta_H\rangle$; as expected this is larger in the model complexes than in the protein samples. Table IV and Figure 9a show that for the tyrosinate model complexes $\theta_\alpha \approx 0°$, which is expected since this minimizes steric hindrance. For both protons $|\theta_H| \approx 60°$ so that the shifts of the two protons are similar, and both are shifted less than the meta protons. The small values of θ_α are similar to the 1.4–4.6° values deduced by EPR for radicals of tyrosine and 3,4-dihydroxyphenylalanine in aqueous solution at pH 9.5.[45] However, for uteroferrin $|\theta_\alpha| \approx 20°$; this results in one proton with $|\theta_H| \approx 80°$ (nearly coplanar with the phenyl ring), which is only slightly shifted, and one proton with $|\theta_H| \approx 40°$, which gives rise to peak a. This geometry is shown in Figure 9b. Similar deviations of θ_α from 0° have been deduced from EPR hyperfine couplings in tyrosyl radicals of *Escherichia coli* and bacteriophage T4-induced ribonucleotide reductases ($|\theta_\alpha| \approx 30$ and 20°, respectively)[46,47] and of bacterial photosynthetic reaction centers ($|\theta_\alpha| \approx 13°$),[48] and presumably arise from steric strain imposed by the tertiary structure of the protein. For uteroferrin θ_α increases when oxoanions bind, with larger oxoanions (MoO_4^{2-} and WO_4^{2-}) causing the greater change. The anomalously large temperature dependence ($[-(d\delta/dT)/(\delta^*/T)]$ of Table I) of peak a can be ascribed to a temperature-dependent change in θ_α.

On the basis of the forgoing considerations and the peak integrations, peaks a, c, d, j, and y are assigned to a single tyrosine bound to the ferric ion in uteroferrin. No other set of NMR peaks can be assigned to a second tyrosine ligating either iron(III) or iron(II) (see Figure 7). This refutes earlier speculation[5,16] that two tyrosines were bound to the iron(III) based on the large 4000 M^{-1} cm^{-1} visible extinction coefficient of Uf_r. Recently, the complex $[(hdpFe)_2(\mu\text{-}O)(\mu\text{-}O_2CCF_6H_5)]^+$, where Hhdp is (2-hydroxybenzyl)bis(2'-pyridylmethyl)amine, has been shown to exhibit a visible extinction coefficient of 6600 M^{-1} cm^{-1}, or 3300 M^{-1} cm^{-1} per phenolate bound to iron(III).[49] Thus it appears that factors other than the number of tyrosines bound to each iron can affect the observed extinction coefficients, so that extinction coefficients are not reliable indicators of the number of tyrosines bound to iron(III).

Possible Assignments for Remaining Resonances. Peaks f–i and x remain unassigned, but the magnitude of the shifts and the r_{eff} values suggested by the T_1 values indicate that these resonances (with the possible exception of x) are shifted by a contact mechanism and, hence, belong to protons on functional groups ligating the dinuclear iron center of uteroferrin. Other resonances observed between −10 and +20 ppm may be due to dipolar shifts of protons of nonligating amino acids 4.5–6 Å from the ferrous ion. We note that there are no peaks in the downfield region with $r_{eff} < 5$ Å; thus, none of the downfield-shifted resonances correspond to the ortholike protons of imidazole ($r_{eff} \approx 3.5$ Å) or to the CH_2COO^- protons of a bridging carboxylate ($r_{eff} \approx 4.5$ Å). It is likely that these resonances do occur in the downfield region, but they would be broad and be obscured by the sharper peaks and the base-line roll.

We propose tentative assignments for resonances f–i that are *consistent with* (but not *implied by*) the observed δ and T_1 values and that involve amino acid ligands to iron that are precedented in metalloproteins. Values of r_{eff} for f–i average 5.3, 5.7, 5.5, and 6.0 Å, respectively, and are consistent with meta protons of tyrosine or histidine (Figure 7). However, assignment of any of these peaks to meta protons of a second coordinated tyrosine is ruled out because no peaks besides a and j are observed with T_1 values long enough to arise from a tyrosine methylene, and at least one such peak should be observed with $\delta_{con} > 0.6\ \delta_{con}$(meta).

Assignment of any of these peaks to the metalike CH of an imidazole coordinated to Fe(III) is also ruled out, because none of these peaks have δ_{con} values of >50 ppm. In model compounds, the shift of the m-CH of an imidazole in an iron complex is found to be comparable to but slightly smaller than that of the m-NH (Table III). In the case of Uf_r, the m-CH of an Fe(III)-bound histidine would be expected near 70 ppm. Its absence strongly suggests that the histidine coordinated to the Fe(III) is bound through N_ϵ. The β-CH_2 protons of such an N_ϵ-coordinated histidine should be observed near 20 ppm (Table III and Figure 7). The peaks h and i both have appropriate shift and r_{eff} values for such an assignment. This assignment would explain the relatively constant average of δ for peaks h and i, while the variability of the spacing between peaks h and i in the different forms of uteroferrin would be due to changes in the torsion angles about the C_β–C_γ bond. The shifts observed for h and i are those expected for $|\theta_H| \approx 30°$.

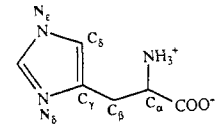

Similar considerations affect the shift of the metalike CH of imidazole bound to Fe(II) (Table III and Figure 7). Thus, peak f or g has suitable shift and r_{eff} values for assignment to the m-CH of an Fe(II)–histidine, but both cannot be due to such a proton, unless the N_ϵ H of one such histidine was in fast exchange with the solvent (and thus NMR-silent). Such an assignment for f or g would imply then that the histidine coordinated to Fe(II) is bound through N_δ. β-CH_2 protons of such a histidine would probably be too broad to be observed ($r_{eff} \approx 3.5$ Å if the dihedral angle C_α–C_β–C_γ–N_δ for His is 180°).

Peaks f and g may alternatively be assigned to one or both of β-CH_2 or γ-CH_2 protons of a terminally coordinated aspartate or glutamate, respectively. Their T_1 (r_{eff}) values are consistent with an Fe(II)-coordinated carboxylate, and their δ values are close to the 31 ppm value found for the acetate methyl resonance in $[Fe^{II}Zn^{II}(bpmp)(OAc)_2]BPh_4$,[50] which serves as a reasonable model for carboxylates bound only to Fe(II). It is likely that

(44) Derbyshire, W. *Mol. Phys.* **1962**, *5*, 225–231.
(45) Sealy, R. C.; Harman, L.; West, P. R.; Mason, R. P. *J. Am. Chem. Soc.* **1985**, *107*, 3401–3406.
(46) Sjöberg, B.-M.; Reichard, P.; Gräslund, A.; Ehrenberg, A. *J. Biol. Chem.* **1978**, *253*, 6863–6865.
(47) Sahlin, M.; Gräslund, A.; Ehrenberg, A.; Sjöberg, B.-M. *J. Biol. Chem.* **1982**, *257*, 366–369.
(48) Barry, B. A.; Babcock, G. T. *Chem. Scr.* **1988**, *28A*, 117–122.
(49) Yan, S.; Que, L., Jr.; Taylor, L. F.; Anderson, O. P. *J. Am. Chem. Soc.* **1988**, *110*, 5222–5224.
(50) Holman, T. R., unpublished observations.

torsion angles influence the isotropic shifts of the CH_2 protons as they do in tyrosine and histidine ligands. If both $\theta_H \approx 30°$, peaks f and g could arise from the same CH_2 group; alternatively, one carboxylate CH_2 proton could give rise to peak f or g ($\theta_H \approx 30°$) and the other CH_2 proton could be buried in the diamagnetic region of the spectrum ($\theta_H \approx 90°$).

Exchangeable peak x cannot be assigned to a ligand on the dinuclear unit, since none of the potential iron ligands are expected to have upfield exchangeable resonances. Peak x and an r_{eff} of ca. 4.5 Å may arise from a nearby NH proton, which experiences a dipolar shift from the Fe(II) atom. Such a distance is estimated to give rise to a $\delta_{dip} \approx -23$ ppm, which is consistent with our observations, given the uncertainty of the calculations.

Conclusions

The NMR spectrum of uteroferrin contains paramagnetically shifted resonances, which have been assigned to a tyrosine (peaks a, c, d, j, and y) and histidine (peaks b and, probably, h and i) bound to iron(III) and to a histidine bound to iron(II) (peaks e and, probably, f). Peak g is proposed to arise from one of the CH_2 protons of a carboxylate ligated to iron(II), and peak x may arise from an uncoordinated NH ca. 4.5 Å away from the Fe(II) center. These assignments have relied on both chemical shift arguments and an analysis of T_1 relaxation times using Solomon–Bloembergen equations modified to account for the effects of the coupled dinuclear center as well as ligand-centered dipolar relaxation. The validity of this approach was verified by analysis of $[(bpmp)Fe_2(OPr)_2]^{2+}$.

Bridging ligands are not observed by NMR because of the proximity of the protons to both spin centers, but the existence of at least two bridging ligands can be inferred from the short Fe–Fe separation (and small Debye–Waller factor, indicating little vibrational variation in this distance) determined by EXAFS.[34,35] The presence of a one-atom (O^{2-} or HO^-) bridge in uteroferrin is supported by the magnitude of J, which is similar to that of semimethemerythrin azide, which is thought to contain a hydroxide bridge.[51] The presence of additional bridges is supported by the short Fe–Fe separation. Although methemerythrin, the prototype of this class of proteins, has two additional carboxylate bridges,[52] recent model studies show that one additional carboxylate bridge is sufficient to constrain the Fe–Fe distance to the values observed for these proteins.[49] Thus, we propose the following model for the dinuclear site of uteroferrin:

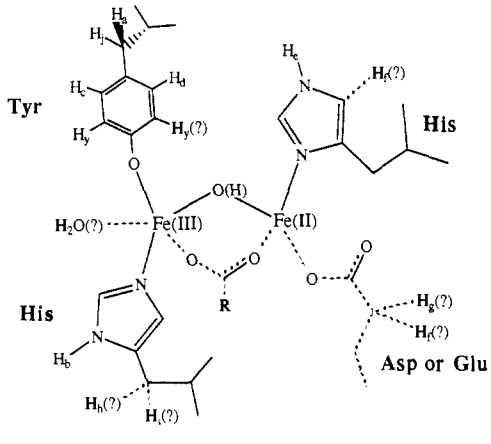

Peak assignments that are consistent with the data but remain ambiguous are indicated by question marks, while ligands that have not been independently corroborated are shown with dashed lines. We also show only one bridging carboxylate for simplicity.

The apparent catalytic role of the metal center in phosphatase activity suggests the presence of vacant or solvent coordination sites in Uf_r. Indeed electron spin echo envelope modulation studies demonstrate the coordination of molybdate to the dinuclear center in Uf_r, although it cannot be deduced to which metal center(s) the anion coordinates.[28] Furthermore, EXAFS studies of the phosphate complexes of both oxidized bovine and porcine enzymes implicate the presence of a bridging phosphate.[34,35] The addition of molybdate, tungstate, or arsenate to Uf_r causes only slight changes in the positions of the various resonances, indicating that none of the NMR-observable amino acid ligands are displaced from the dinuclear cluster. The addition of phosphate, on the other hand, causes more dramatic changes. At pH 4.9 the NMR spectrum of Uf_rPO_4 is obliterated for reasons that are not understood,[26] while that at pH 3 exhibits shifts and temperature dependences indicative of weaker antiferromagnetic coupling ($-2J \ll 20$ cm^{-1}). The latter is consistent with the $2J$ value of -6 cm^{-1} found from magnetic susceptibility studies of Uf_rPO_4 at pH 4.9.[11]

The substantial decrease in J upon phosphate binding suggests an alteration of the single-atom bridge that weakens the antiferromagnetic interaction between the metal centers in the dinuclear cluster. One possibility (suggested by reviewer) is that the phosphate replaces the hydroxo bridge. Such a substitution would certainly be consistent with the weakening of the antiferromagnetic interaction. Wieghardt et al.[53] synthesized complexes of the type $[LFe^{III}(\mu\text{-}XO_2)_3Fe^{III}L]$ with phosphate, arsenate, and molybdate bridges and demonstrated weak antiferromagnetic coupling ($-2J < 9$ cm^{-1}) for these diferric complexes. Coupling in the mixed-valence form would be expected to be weaker. However, in the context of Uf_r–anion interactions where only phosphate causes this decrease in coupling, it is difficult to justify a bridging phosphate in Uf_rPO_4 and a terminal arsenate in Uf_rAsO_4, since the biochemical effects of phosphate and arsenate on Uf_r are so similar, i.e., millimolar K_i's and potentiation of oxidative inactivation. Furthermore, Mössbauer studies on Uf_rPO_4 show that only the Fe(III) center is significantly affected by phosphate binding.[15]

Another possible explanation of the weakened coupling is that the coordination of $H_2PO_4^-$ to the Fe(III) center of Uf_r results in the transfer of one of its protons to the single-atom bridge, thus converting a μ-OH bridge in Uf_r to a μ-H_2O bridge in Uf_rPO_4. The μ-aqua bridge proton may remain hydrogen bonded to the bound phosphate. A similar protonation of the μ-OH bridge of deoxyhemerythrin is proposed to explain the changes observed in the magnetic properties of the dinuclear cluster upon azide binding.[54] Precedence for a water molecule bridging the metal centers of a mixed-valence diiron complex is presently lacking, but μ-aquadimetal(II) complexes are known.[55] Indeed, the terminal carboxylates of the complexes $\{[M(tmen)(O_2CR)]_2(\mu\text{-}H_2O)(\mu\text{-}RCO_2)_2\}$ (M = Co(II), Ni(II); tmen = *N,N,N',N'*-tetramethyl-1,2-diaminoethane) exhibit the hydrogen bonding to the μ-aqua bridge proposed for Uf_rPO_4.

Acknowledgment. This work was supported by grants from the National Science Foundation (DMB-8314935 and DMB-8804458). R.C.S. is grateful for an American Cancer Society Fellowship.

Registry No. Fe(salen)(NAc-Tyr-OMe), 88006-00-2; Fe(salen)(CBZ-Tyr-PNB), 124069-81-4; Fe(salen)(Tyr-OMe), 88006-01-3; AsO_4^{3-}, 15584-04-0; PO_4^{3-}, 14265-44-2; MoO_4^{2-}, 14259-85-9.

Supplementary Material Available: Diagram of the fits of intensity vs τ for $UfMoO_4$ T_1 inversion–recovery data shown in Figure 4 (1 page). Ordering information is given on any current masthead page.

(51) Scarrow, R. C.; Maroney, M. J.; Palmer, S. M.; Que, L., Jr.; Roe, A. L.; Salowe, S. P.; Stubbe, J. *J. Am. Chem. Soc.* **1987**, *109*, 7857–7864.
(52) Stenkamp, R. E.; Sieker, L. C.; Jensen, L. H. *J. Am. Chem. Soc.* **1984**, *106*, 618–622.
(53) Chaudhuri, P.; Winter, M.; Wieghardt, K.; Gehring, S.; Haase, W.; Nuber, B.; Weiss, J. *Inorg. Chem.* **1988**, *27*, 1564–1569. Drücke, S.; Wieghardt, K.; Nuber, B.; Weiss, J.; Fleischhauer, H.-P.; Haase, W. *J. Am. Chem. Soc.* In press.
(54) Reem, R. C.; Solomon, E. I. *J. Am. Chem. Soc.* **1987**, *109*, 1216–1226.
(55) Turpeinen, U.; Hämäläinen, R.; Reedijk, J. *Polyhedron* **1987**, *6*, 1603–1610.